nature geoscience

Article

https://doi.org/10.1038/s41561-025-01756-7

Elevated shallow water salinity in the deglacial Indian Ocean was sourced from the deep

Received: 27 November 2023

Accepted: 26 June 2025

Published online: 06 August 2025

Check for updates

Ryan H. Glaubke[1,7] ✉, Elisabeth L. Sikes[1], Sindia M. Sosdian[2], Natalie E. Umling[1,3], Aidan Starr[1,4], Paola L. Moffa-Sanchez[5] & Matthew W. Schmidt[6]

Along the northern rim of the Southern Ocean, the transformation of upwelled deep waters into less-dense Subantarctic Mode Waters forms a critical link between the deep and shallow layers of the global ocean. In the Indian sector, mode waters comprise a key component of Agulhas Leakage, which today conveys salt to the Atlantic basin necessary for sustaining deep water formation. The salinity of Indian-sourced mode waters may therefore represent an upstream influence on Atlantic overturning, with implications for global climate. Here we reconstructed the temperature and salinity of these waters across the Last Deglaciation using the geochemistry of two planktic foraminiferal species from a south Indian Ocean sediment core. Approximately 20,000 years ago (~20 ka), deglaciation was marked by an abrupt ~2–2.6 practical salinity unit increase that persisted until ~16 ka. This event coincided with an increase in water mass age reconstructed from the same core. We argue this coherence is evidence for an aged, salty glacial bottom water mass that, once upwelled, modified the salinity of Indian-sourced mode water. Model experiments suggest this salt had the potential, if leaked into the Atlantic, to nudge overturning towards its modern-day configuration, highlighting an underappreciated deep ocean influence on the deglacial dynamics.

The production of Subantarctic Mode Water (SAMW) represents a major pathway for deep waters to become reincorporated into the shallow circulation of the global ocean[1]. Wind-driven divergence around Antarctica brings deep ocean waters to the surface, some of which are advected northward and transformed into less-dense mode and intermediate waters[2,3]. The lightest of these, SAMW, is responsible for renewing thermocline waters throughout the global ocean and represents a key pathway for heat, salt, carbon and nutrients to be transported from high to low latitudes[2,4–6]. SAMW formation begins at the surface in localized 'hotspots' along the northern rim of the Southern Ocean where wintertime cooling, Ekman pumping and eddy activity drives deep mixing[1,7]. One of the largest of these hotspots is the southeast Indian Ocean[8–10] (Fig. 1). Here eddies in the wake of the Kerguelen Plateau mix upwelled deep waters from the Southern Ocean with subtropical surface waters delivered by the Agulhas Retroflection[11] (Fig. 1a). These waters are subducted into the subsurface at the subtropical front (STF)

[1]Department of Marine and Coastal Sciences, Rutgers University, New Brunswick, NJ, USA. [2]School of Earth and Environmental Sciences, Cardiff University, Cardiff, UK. [3]Department of Earth and Planetary Sciences, American Museum of Natural History, New York, NY, USA. [4]Department of Geography, University of Cambridge, Cambridge, UK. [5]Department of Geography, Durham University, Durham, UK. [6]Department of Ocean and Earth Sciences, Old Dominion University, Norfolk, VA, USA. [7]Present address: Department of Geosciences, University of Arizona, Tucson, AZ, USA. ✉e-mail: glaubke@arizona.edu

https://doi.org/10.1038/s41561-025-01756-7

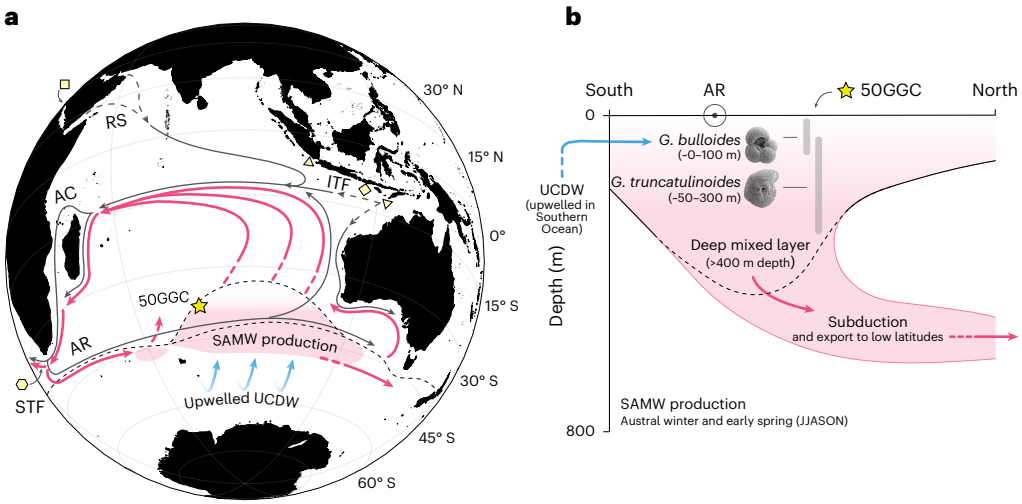

Fig. 1 | SAMW production and circulation in the south Indian Ocean. **a**, A generalized schematic of the region's shallow circulation and major hydrographic features. The major SAMW formation region and its associated circulation at depth (~200–600 m) is coloured red. Upper ocean flows contributing to SAMW formation are coloured grey. Deep ocean sources are coloured blue. Core TT1811-50GGC is marked by a yellow star. Records representing Indonesian Throughflow[61–63], Red Sea (RS) overflow[65] and Agulhas Leakage[67] in Fig. 4 are represented by pale yellow symbols (Fig. 4 caption). Major currents, water masses and hydrographic features are labelled accordingly: Agulhas Current (AC), Agulhas Retroflection (AR), ITF, SAMW, STF and upper-Circumpolar Deep Water (UCDW). **b**, A generalized schematic of the upper water column during SAMW production (June–November). The depth preferences of *G. bulloides* and *G. truncatulinoides* are indicated by the vertical grey bars, according to refs. 41,42. Colours and water mass abbreviations correspond to those in **a**. Panel **a** inspired by refs. 8–10,72–74 and adapted with permission from ref. 50, Elsevier. *G. truncatulinoides* image adapted from ref. 75, Micropaleontology. Credit: *G bulloides* image, Lucia de Abreu.

before flowing northward within the shallow interior (~200–600 m) of the subtropical gyre[12] (Fig. 1b). This subsurface flow is substantial, rivalling the volume transport of the basin's largest supply of upper ocean waters, the Indonesian Throughflow (ITF; ~12–14 Sv versus ~15 Sv, respectively; 1 Sv = 1×10^6 m^3 s^{-1})[4,10,13,14]. SAMW then steers westward towards the African continent where it coalesces with other source waters into a collection of distinct southerly flows[15] comprising the basin's major western boundary current, the Agulhas Current[11] (Fig. 1a).

As the Agulhas overshoots the southern tip of Africa, approximately half of its volume transport above 1,000 m 'leaks' into the South Atlantic as mesoscale eddies[11]. These eddies entrain ~13–26% of newly formed Indian SAMW[4,11], supplying the bulk of all mode waters crossing the equatorial Atlantic to deep convection sites farther north[4,16,17]. Today, Agulhas Leakage is considered an important source of salt necessary for maintaining deep water production in the North Atlantic[18]. Previous studies have suggested that on glacial–interglacial timescales, variability in leakage volume, mediated by migrations of the STF, probably affected convection strength and, by extension, the configuration of the Atlantic overturning circulation[19–25]. Additionally, changes in the salt content of Leakage itself, linked to upstream changes in Indian source waters, has been identified as a potential influence on circulation[26–28]. These findings underscore the importance of constraining the salinity histories of Indian-sourced thermocline waters to better understand their influence on overturning and global climate.

Among these, SAMW is central due to the role the deep ocean plays in its formation (Fig. 1). During the Last Glacial Maximum (LGM; ~23–19 thousand years ago (ka)), the salinity of the deep ocean increased by ~1.4–3 practical salinity units (PSU)[29–31], a likely response to increased brine rejection during Antarctic Bottom Water (AABW) formation across a broader Antarctic sea ice cap[32]. The presence of this salt increased the density stratification between northern-sourced deep waters and southern-sourced bottom waters[29,32], resulting in two largely independent overturning cells that stand in contrast to the more interconnected circulation of the ocean today[2,33]. Isolating the abyssal glacial ocean from the atmosphere allowed remineralized carbon from sinking organic material to accumulate and age in the ocean interior[34]. The breakdown of this stratification during the Last Deglaciation (~18–11 ka) allowed carbon-rich deep waters to upwell throughout the Southern Ocean and release CO_2 to the atmosphere[35], warming the planet. These waters then recirculated into the ocean's shallow interior, as evidenced by transient depletions in the radiogenic (^{14}C) and stable isotope composition of carbon (^{13}C) in fossil subsurface-dwelling foraminifera from low-latitude sediment cores[36–40]. We should expect the salinity that helped form this abyssal carbon reservoir would upwell alongside deep ocean-sequestered CO_2, providing an acute source of salt to the ocean's shallow circulation. However, evidence for upwelled abyssal ocean salt remains elusive.

Here we reconstruct the temperature and salinity of incipient SAMW from the southeast Indian Ocean by combining magnesium–calcium (Mg/Ca) palaeotemperature estimates with ice volume-corrected stable oxygen isotope values (δ^{18}O) from two planktic foraminiferal species (*Globigerina bulloides* and *Globorotalia truncatulinoides*). Analyses were conducted on sediment core TT1811-50GGC (hereafter 50GGC; 38.3° S, 77.7° E, 1,118 m) raised from the Île Amsterdam–Île St Paul Plateau within the southeast Indian Ocean's extensive SAMW formation region (Fig. 1a). Our location is ideally suited to examine hydrologic changes in Indian SAMW at its point of origin (Fig. 1a), whereas the depth and seasonal growth preferences of *G. bulloides* (upper ~100 m; early spring)[41] and *G. truncatulinoides* (~50–300 m; late fall/winter)[42] ensures we index upper ocean conditions during active SAMW formation[10] (Fig. 1b). Altogether, our new data illustrate SAMW as a potential pathway for the deep ocean to influence deglacial overturning.

Deglacial changes in SAMW temperature and salinity

The geochemical data from both species reveal typical glacial–interglacial trends, with more enriched δ^{18}O and lower Mg/Ca ratios characterizing the LGM relative to the Holocene (Fig. 2a,b). Deglacial warming is marked by a 0.6 and 0.3 mmol mol^{-1} increase in Mg/Ca for *G. bulloides* and *G. truncatulinoides*, respectively, beginning at ~20 ka (Fig. 2a). This timing mirrors early warming signals found in marine

https://doi.org/10.1038/s41561-025-01756-7

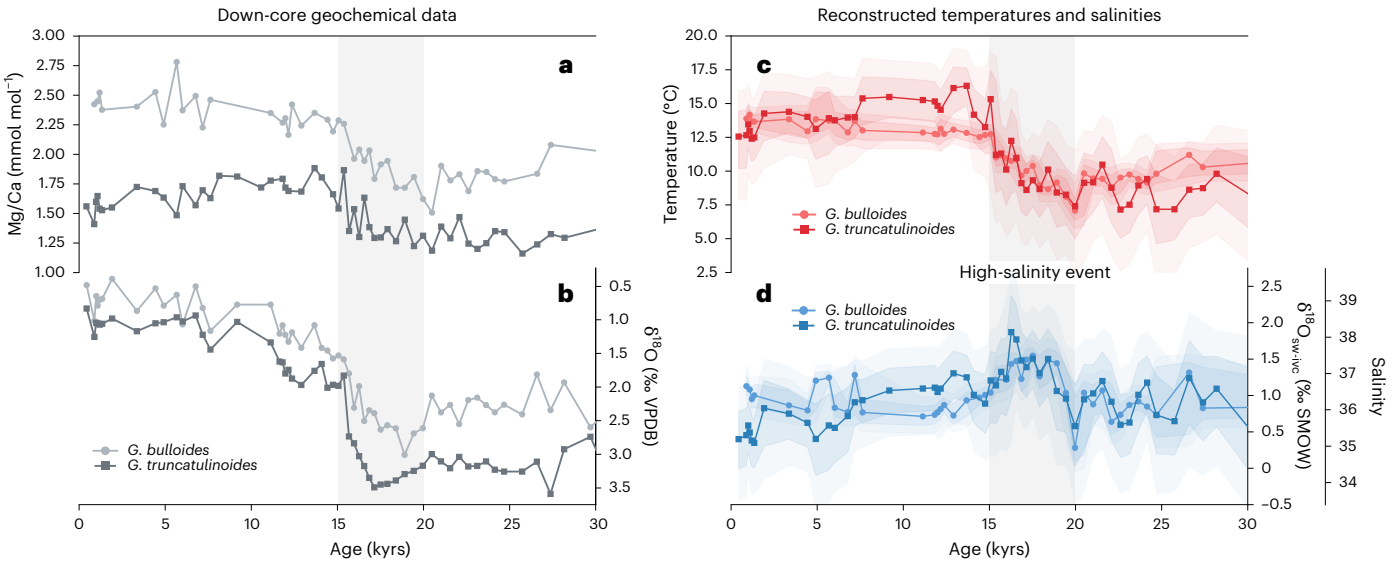

Fig. 2 | Temperature and salinity reconstructions from *G. bulloides*, circles, and *G. truncatulinoides*, squares, from core 50GGC. a,**b**, Raw Mg/Ca (**a**) and stable oxygen isotope (**b**) records over the last 30 ka. Note the *y* axis for the oxygen isotope values in **b** is reversed. **c**,**d**, Estimated temperatures (red; **c**) and ice volume-corrected oxygen isotope values ($\delta^{18}O_{sw\text{-}ivc}$; blue; **d**) derived from the data in **a** and **b**. A secondary *y* axis in **d** shows the conversion from $\delta^{18}O_{sw\text{-}ivc}$ to absolute salinity (Methods). The markers represent the nominal temperature and salinity estimates derived from the geochemical data, whereas the transparent envelopes represent Monte-Carlo-derived uncertainties (1σ and 2σ). Grey vertical bars in **c** and **d** represent the general timing of the high-salinity event.

records throughout the Southern Hemisphere mid-latitudes[43]. Meanwhile, the $\delta^{18}O$ data show a depletion from the LGM to the Holocene of 1.61‰ and 2.16‰ for *G. bulloides* and *G. truncatulinoides*, respectively (Fig. 2b), reflecting the net effect of changing ocean temperature, global ice volume and local salinity[44]. Given the strong temperature influence on foraminiferal $\delta^{18}O$, we should expect the excursion towards more depleted $\delta^{18}O$ to coincide with the rise in Mg/Ca, all else being equal. However, both $\delta^{18}O$ records initially grow more enriched as Mg/Ca increases, increasing by 0.92‰ and 0.52‰ for *G. bulloides* and *G. truncatulinoides*, respectively, before transitioning to depleted values later in the deglaciation (Fig. 2a,b). Only an expansion of global ice volume or an increase in local salinity can explain this mismatch between expected versus observed $\delta^{18}O$ behaviour. Because records of eustatic sea level do not suggest a temporary expansion in ice volume at that time[45], the most likely explanation is an increase in salinity.

We quantified salinity changes by correcting the foraminiferal $\delta^{18}O$ records for temperature and ice volume effects (Methods). Mg/Ca ratios from each species were first converted to temperatures using species-specific and, for *G. truncatulinoides*, morphotype-specific calibrations[46,47]. We used relationships determined from culture to remove the thermal component of the $\delta^{18}O$ signal[48] and subtracted the ice volume effect using a high-resolution deglacial sea-level record[49]. The residual ice volume-corrected seawater $\delta^{18}O$ signal ($\delta^{18}O_{sw\text{-}ivc}$) reflects local $\delta^{18}O_{sw}$ variability as an offset from the contemporaneous global mean, which covaries linearly with ocean salinity[44]. We converted $\delta^{18}O_{sw\text{-}ivc}$ to absolute salinities using a regional equation developed from modern observations[50] and applied this relationship consistently down core following model results suggesting the $\delta^{18}O_{sw}$–salinity relationship in this region is relatively stable through time[51]. Analytical and age model uncertainties were propagated throughout using a bootstrapping approach[52] (Methods).

Both foraminiferal species exhibit remarkably similar temperature and salinity histories (Fig. 2c,d), suggesting both capture the same incipient SAMW forming at 50GGC (Fig. 1b and Supplementary Fig. 1). The temperature records show deglacial upper ocean warming of 3.8 ± 0.6 °C and 4.6 ± 1.4 °C (1σ) for *G. bulloides* and *G. truncatulinoides*, respectively. At the onset of warming (~20 ka), both species register

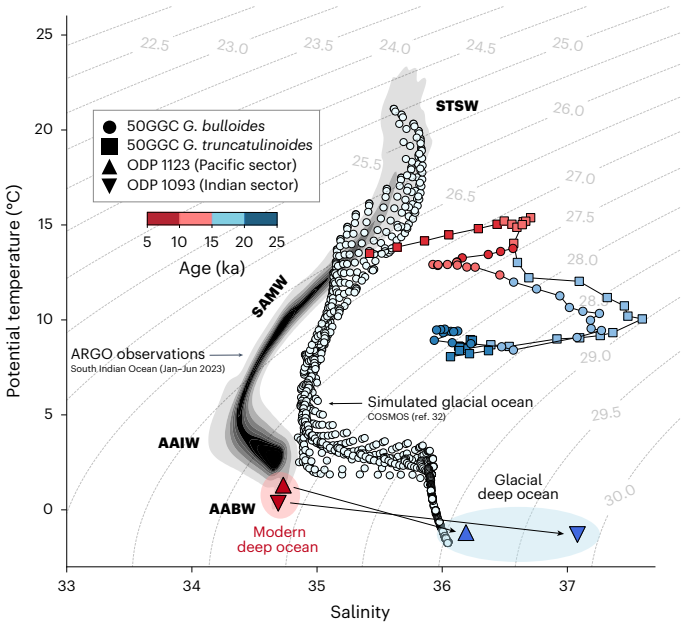

Fig. 3 | A temperature–salinity diagram of modern, glacial, and transient deglacial conditions in the south Indian Ocean. Temperatures and salinities reconstructed from *G. bulloides* (circles) and *G. truncatulinoides* (squares) are low-pass filtered using a Savitsky–Golay filter to highlight long-term trends. Data are binned and coloured by age (colour bar). Greyscale kernel density estimate shows the distribution of modern temperature–salinity observations from Argo floats throughout the south Indian Ocean from January–June 2023 (retrieved using the 'argopy' package for Python[55]). Major water masses are labelled: Subtropical Surface Water (STSW), SAMW, Antarctic Intermediate Water (AAIW) and AABW. Light blue dots represent temperature–salinity values for the glacial ocean simulated by the climate model COSMOS[32]. Triangles represent modern (red) and glacial bottom water salinities (blue) estimated from pore-water chlorinity profiles in Ocean Discovery Program (ODP) sediment cores in the Indian and Pacific sectors of the Southern Ocean[29]. Light grey contours represent lines of constant density (in kg m^{-3}).

https://doi.org/10.1038/s41561-025-01756-7

an abrupt 1.0 ± 0.2‰ to 1.2 ± 0.3‰ increase in $\delta^{18}O_{sw\text{-}ivc}$ that remains enriched relative to glacial values until ~16.2 ka, equating to a salinity increase of 2.0 ± 0.4 PSU to 2.6 ± 0.9 PSU. Although salinity has been shown to influence Mg/Ca-based temperature estimates[53,54], the lack of a substantial change in Mg/Ca ratios during this high-salinity event suggests this potential bias is minor (Fig. 2a,b). More importantly, the presence of high salinities in records from two foraminiferal species, determined from two independent systems of equations, suggests this event is a robust feature of the region's palaeoceanographic history.

The magnitude of the estimated salinity increase is anomalous for upper ocean waters relative to both modern and glacial conditions (Fig. 3). Before ~20 ka, reconstructed temperature–salinity values at our location suggest SAMW was somewhat saltier and denser than today, according to Argo observations from the region[55]. After ~20 ka, the data's trajectory towards higher salinities exceeds that of glacial SAMW simulated by the global climate model COSMOS[32], increasing upper ocean density by ~0.8–1 kg m^{-3}. These waters could not reside in the upper mixed layer in the modern ocean without destabilizing the water column. However, temperature–salinity values from the glacial ocean simulation show that the underlying intermediate and deep waters were also much denser, providing a dynamically stable water column that, with deglacial wind shifts and intensification, could entrain this salt into Indian SAMW.

The question remains: where did this salt come from?

The deep origin hypothesis

The magnitude of the SAMW salinity estimates at the peak of the high-salinity event resemble glacial bottom water salinities reconstructed from pore-water chlorinity profiles in the Indian and Pacific sectors of the Southern Ocean[29] (Fig. 3). This resemblance raises the possibility that SAMW salinities at our location were modified by a deep, highly saline water mass after it was upwelled in the Southern Ocean during the Last Deglaciation. The most compelling evidence in support of this argument comes from old water mass ages recorded by the radiocarbon content of planktic (*Globoratalia inflata*) and benthic foraminifera (*Cibicidoides wuellerstorfi*) in the same core[56]. The radiocarbon records show an ~3,000-yr increase in upper ocean water mass age that occurs synchronously with rising salinities at ~20.2–20.3 ka, according to a changepoint analysis[57] (Methods, Fig. 4b,g and Table 1). Because both records are based on co-registered samples, this synchroneity is independent of age model considerations. The correspondence between salt and radiocarbon offers forceful support that both

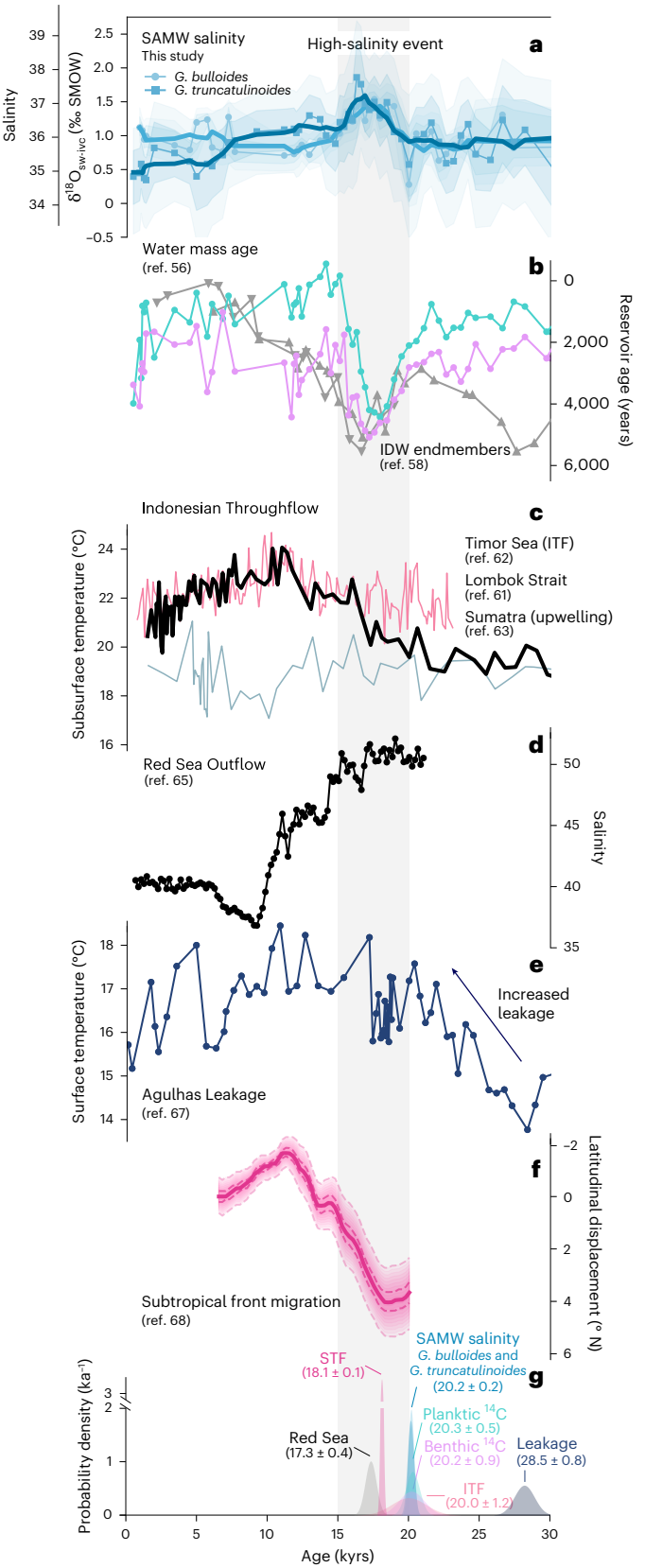

Fig. 4 | Comparison of the salinity signal at 50GGC with reconstructed changes in deep ocean upwelling, low-latitude water mass sourcing and Southern Ocean frontal migration. a, Reconstructed salinities from *G. bulloides* (circles; light blue) and *G. truncatulinoides* (squares; dark blue) at 50GGC. **b**, Reconstructed water mass ages from *G. inflata* (green) and *C. wuellerstorfi* (purple) at 50GGC[56]. Dark grey records represent water mass ages from cores SS172–4040 (triangles; 2,788 m) and SS152–3828 (inverted triangles; 3,166 m) from the equatorial Indian Ocean[58], which today capture IDW. **c**, Subsurface temperature records from thermocline-dwelling foraminifera from the Timor Sea[62], Lombok Strait[61] and Sumatran coastal upwelling system[63] (marked as inverted triangle, diamond and triangle, respectively, in Fig. 1a). **d**, Reconstructed salinities from the northern Red Sea[65] (marked as square in Fig. 1a). **e**, Surface temperatures from the Agulhas Bank derived from *G. bulloides* Mg/Ca ratios in the Agulhas Bank Splice[67] (marked as hexagon in Fig. 1a). **f**, A record of STF migration derived from a compilation of stable oxygen isotope records spanning the Indo-Pacific sector of the Southern Ocean[68]. Median estimates (solid hot pink line) are plotted alongside a cumulative probability density (light pink colouring) with ±1σ and ±2σ bounds (dashed hot pink line). **g**, Changepoint estimates identifying the onset of deglacial changes in SAMW salinity, water mass age, subtropical source water supply/salt content and frontal migration. The *y* axis was broken because the magnitude of the STF changepoint flattens the others, making them difficult to see. Changepoints estimated using a piecewise regression approach[57]. Distributions represent 95% confidence limits from n = 5,000 Monte Carlo realizations. Each distribution is labelled with its nominal breakpoint and ±1σ error. The dark vertical grey bar indicates the general timing of the high-salinity event in 50GGC. A comparison of each records' respective age model can be found in Supplementary Fig. 5.

https://doi.org/10.1038/s41561-025-01756-7

Table 1 | Changepoint estimates and two-tailed *z*-test results from pairwise changepoint comparisons

Record	Ref.	Changepoint (ka)	Compared to:			
			SAMW salinity (*G. bulloides*)	SAMW salinity (*G. truncatulinoides*)	SAMW age (planktic)	SAMW age (benthic)
SAMW salinity (*G. bulloides*)	This study	20.2±0.2	—			
SAMW salinity (*G. truncatulinoides*)	This study	20.2±0.2	z=0.25 P=0.80	—		
SAMW water mass age (planktic)	56	20.3±0.5	z=−0.43 P=0.66	z=−0.58 P=0.56	—	
SAMW water mass age (benthic)	56	20.2±0.9	z=−0.06 P=0.95	z=−0.14 P=0.89	z=0.15 P=0.88	—
Indonesian Throughflow	61	20.0±1.2	z=0.27 P=0.79	z=0.21 P=0.84	z=0.42 P=0.68	z=0.26 P=0.80
Red Sea Outflow	65	17.3±0.4	**z=18.7 P=1.13×10^{-78}**	**z=17.6 P=2.81×10^{-69}**	**z=12.0 P=3.12×10^{-33}**	**z=6.26 P=3.66×10^{-10}**
Agulhas Leakage	67	28.2±0.7	**z=−18.9 P=1.48×10^{-79}**	**z=−18.8 P=3.26×10^{-79}**	**z=−16.9 P=1.91×10^{-64}**	**z=−13.1 P=1.74×10^{-39}**
Subtropical Front Migration	68	18.1±0.1	**z=19.1 P=3.58×10^{-81}**	**z=17.0 P=7.74×10^{-65}**	**z=9.80 P=1.11×10^{-22}**	**z=4.70 P=2.63×10^{-6}**

Results significant at the 95% confidence threshold (P<0.05) are bolded.

anomalies were delivered to our study location by the same signal carrier: upwelled deep ocean waters.

Importantly, the deglacial radiocarbon data from 50GGC align with benthic reservoir ages from two mid-depth sediment cores in the equatorial Indian Ocean[58] (Fig. 4b). This agreement suggests that the route aged, salty bottom waters took to escape the abyss involved Indian Deep Water (IDW) formation. In the modern ocean, IDW is formed at mid-depths through diapycnal mixing of AABW with warmer overlying waters[59], which increases its buoyancy and provides a low-latitude closure between the upper and lower cells of the overturning circulation. IDW returns to the Southern Ocean as UCDW, where it is upwelled by the winds and advected northward at the surface to feed SAMW production[2] (Fig. 1). During the LGM, when stronger stratification isolated the upper and lower cells, this pathway was cut off. Instead, IDW recirculated within the ocean interior and accumulated respired carbon, like what has been observed in the Pacific[59,60]. We suggest that early mid-latitude warming would have provided the increased wind stress and surface buoyancy forcing necessary to enhance interior ocean mixing, eroding deep-sea stratification and re-establishing the connection between AABW, IDW/UCDW and SAMW that exists today[1,2]. This switch to the modern ocean's more interconnected configuration opened an escape hatch for these saline deep waters to upwell and modify SAMW salinity.

Deglacial SAMW salinity change was not driven by upper ocean sources

Alongside upwelled deep waters, subtropical surface waters from the Indonesian and Red seas (among other marginal inputs) advected by the Agulhas Retroflection are important ingredients for SAMW formation[11] (Fig. 1a). Upstream changes in the supply/composition of these waters may, in theory, offer an alternative explanation for the high-salinity event. We compiled representative records for each of these source waters and, using changepoint analyses and *z*-score significance testing (Methods), find that they cannot fully explain the salinity signal at 50GGC (Fig. 4 and Table 1).

Deglacial subsurface temperature records from the outlet of the ITF—a source of relatively fresh water to the Indian Ocean[11]—show no abrupt reduction in volume during the Last Deglaciation that could have increased salinity at 50GGC[61–63] (Fig. 4c). Instead, at the same time as the high-salinity event (20.0 ka; z = 0.27 and 0.21; P = 0.84 and 0.79), subsurface temperatures in the Lombok Strait began to shift away from conditions typical of the nearby Sumatran upwelling system and towards those resembling the Timor Sea, an indicator of increasing ITF flow[61] (Fig. 4c,g). If Indian SAMW was substantially influenced by changes in the ITF during the Last Deglaciation, we would expect this intensification to freshen waters at our core site. We observe the opposite, arguing against an ITF influence.

In the glacial Red Sea, waters were especially saline owing to high evaporation and limited open ocean exchange due to lower sea levels[64]. Rising seas during the Last Deglaciation could have released this salt into the Agulhas Current, impacting our core site downstream. However, a local salinity reconstruction suggests these waters did not begin flushing into the Indian Ocean until 17.3 ka (ref. 65; Fig. 4d,g), too late to be a viable explanation for the salinity increase at 50GGC (z = 18.7 and 17.6; P < 0.001).

Restrictions of Agulhas Leakage across the Last Deglaciation could also have increased SAMW salinity by strengthening the Agulhas Retroflection and diverting more subtropical waters towards our site[66]. However, surface temperatures from the Agulhas Bank suggest Agulhas Leakage steadily strengthened throughout the Last Deglaciation beginning as early as 28.2 ka (ref. 67; Fig. 4e,g), significantly earlier than the high-salinity event at 50GGC (z = −18.9 and −18.8; P < 0.001). This would have freshened waters at 50GGC. Whereas the timing on leakage intensification varies between available records[19,20], none show an abrupt closure across the Last Deglaciation that would be required to increase the salinity of local SAMW.

Additionally, our core location's proximity to the STF raises the possibility that a deglacial poleward migration of the front could have exposed our study site to saltier subtropical surface waters, increasing local salinity. Nevertheless, a compilation of planktic $\delta^{18}O$ records spanning the Indo-Pacific sector of the Southern Ocean indicates the STF did not begin migrating poleward until ~18.1 ka (ref. 68; Fig. 4f,g), several millennia after the high-salinity event (z = 19.1 and 17.0; P < 0.001). The nearly identical planktic and benthic radiocarbon ages in the deglacial section of 50GGC (Fig. 4b) are also characteristic of subantarctic waters and stand in contrast to the strong vertical gradients in reservoir age observed in subtropical waters[69]. We would also expect a corresponding temperature response that mirrors the

structure and timing of the high-salinity event. Both species show no such feature (Fig. 2c).

In short, changes in upper ocean source waters and frontal position cannot explain the salinity signal at 50GGC. Instead, salinity's coeval behaviour with radiocarbon content, a distinctive geochemical tracer of abyssal waters, strongly implicates a deep ocean origin.

Implications for global ocean circulation

After formation, most Indian SAMW remains within the basin, becoming one of several important source water components to Agulhas Leakage[11] (Fig. 1a). It follows that any modification of SAMW by saline deep waters during the Last Deglaciation would have increased the amount of salt delivered to the Atlantic, an important ingredient for the recovery of a weakened glacial overturning circulation[26,27].

Could the salinity increase at 50GGC, if fully incorporated into SAMW and leaked to the Atlantic, be sufficient to influence overturning strength? We compare our results with two novel 'saltwater hosing' experiments performed with the global climate model COSMOS where freshwater is removed from Agulhas Leakage to increase the salt load to the Atlantic Ocean and, ultimately, force a response in overturning[27,70]. In these experiments, removing 0.05 and 0.1 Sv of freshwater from the surface ocean south of Africa sufficiently increased Agulhas Leakage salinity to reinvigorate deep water production within a few centuries. For comparison, we estimated the equivalent negative freshwater forcing required to achieve the salinity increase observed at 50GGC using a simple reverse dilution equation (Methods; errors represent 1σ uncertainty). For *G. bulloides*, the salinity increase from 36.1 ± 0.5 PSU during the glacial (20–30 ka) to 37.1 ± 0.3 PSU during the high-salinity event (16–18 ka) is equivalent to removing ~0.36 ± 0.18 Sv of freshwater from SAMW, assuming constant production (here we assume a production rate of 11.7 Sv (ref. 71); we explore other rates in the Supporting Information). The same calculation with *G. truncatulinoides* salinities gives a comparable result (0.41 ± 0.26 Sv). Consequently, modified deglacial SAMW would have to comprise ~14 ± 7% (~12 ± 7% for *G. truncatulinoides*) of Agulhas Leakage waters to provide a salt load capable of re-invigorating Atlantic overturning, according to the 0.05 Sv removal experiment[27]. This estimate closely aligns with the proportion of new SAMW that contributes to the Agulhas Leakage today (~13–26%)[4].

These calculations suggest that the injection of saline deep waters into the upper ocean—in addition to a decrease in deep ocean density associated with the breakdown of deep-sea stratification—could have decreased the density difference between the surface and deep enough to promote convection in the North Atlantic. Upwelled glacial deep waters may therefore have provided an overlooked yet potentially important control on the strength of Atlantic overturning in the Last Deglaciation. With the pace and timing of deglacial deep water upwelling governed by changes in the position and intensity of the Southern Hemisphere southwesterly winds[68], our results add to the growing consensus that the Southern Ocean plays an active, rather than passive, role in the dynamics of the Last Deglaciation[43].

Conclusions

Our new temperature and salinity records from a sediment core in the southeast Indian Ocean clarifies the influence of upwelled deep ocean waters on SAMW salinity during the Last Deglaciation. Our data reveal an ~2–2.6-PSU increase in upper ocean salinity between ~20–16 ka. Radiocarbon analyses from the same core[56] show a substantial coeval increase in water mass age. We argue this coherence reflects the upwelling of an aged and highly saline deep water mass that accumulated both salt and remineralized carbon while it was isolated from the atmosphere throughout the last Ice Age[29,32,34]. This water was a substantial salt source to the subtropical Indian Ocean with the density potential to reinvigorate deep water production in the North Atlantic via the Agulhas Leakage[27]. Our results emphasize the importance of Southern Ocean dynamics in facilitating the last major example of global-scale climate change.

Online content

Any methods, additional references, Nature Portfolio reporting summaries, source data, extended data, supplementary information, acknowledgements, peer review information; details of author contributions and competing interests; and statements of data and code availability are available at https://doi.org/10.1038/s41561-025-01756-7.

References

1. Rintoul, S. R. The global influence of localized dynamics in the Southern Ocean. *Nature* **558**, 209–218 (2018).
2. Talley, L. D. Closure of the global overturning circulation through the Indian, Pacific, and Southern oceans: schematics and transports. *Oceanography* **26**, 80–97 (2013).
3. Marshall, J. & Speer, K. Closure of the meridional overturning circulation through Southern Ocean upwelling. *Nat. Geosci.* **5**, 171–180 (2012).
4. Sloyan, B. M. & Rintoul, S. R. Circulation, renewal, and modification of Antarctic Mode and Intermediate water. *J. Phys. Oceanogr.* **31**, 1005–1030 (2001).
5. Sarmiento, J. L., Gruber, N., Brzezinski, M. A. & Dunne, J. P. High-latitude controls of thermocline nutrients and low latitude biological productivity. *Nature* **427**, 56–60 (2004).
6. Sabine, C. L. et al. The oceanic sink for anthropogenic CO_2. *Science* **305**, 367–371 (2004).
7. Sallée, J.-B., Speer, K., Rintoul, S. & Wijffels, S. Southern Ocean thermocline ventilation. *J. Phys. Oceanogr.* **40**, 509–529 (2010).
8. Sallée, J.-B., Wienders, N., Speer, K. & Morrow, R. Formation of Subantarctic Mode Water in the southeastern Indian Ocean. *Ocean Dynam.* **56**, 525–542 (2006).
9. Koch-Larrouy, A., Morrow, R., Penduff, T. & Juza, M. Origin and mechanism of Subantarctic Mode Water formation and transformation in the southern Indian Ocean. *Ocean Dynam.* **60**, 563–583 (2010).
10. Li, Z., England, M. H., Groeskamp, S., Cerovečki, I. & Luo, Y. The origin and fate of Subantarctic Mode Water in the Southern Ocean. *J. Phys. Oceanogr.* https://doi.org/10.1175/jpo-d-20-0174.1 (2021).
11. Durgadoo, J. V., Rühs, S., Biastoch, A. & Böning, C. W. B. Indian Ocean sources of Agulhas Leakage. *J. Geophys. Res. Oceans* **122**, 3481–3499 (2017).
12. Jones, D. C. et al. How does Subantarctic Mode Water ventilate the Southern Hemisphere subtropics? *J. Geophys. Res. Oceans* **121**, 6558–6582 (2016).
13. McDonagh, E. L., Bryden, H. L., King, B. A. & Sanders, R. J. The circulation of the Indian Ocean at 32°S. *Prog. Oceanogr.* **79**, 20–36 (2008).
14. Gordon, A. L. et al. The Indonesian Throughflow during 2004–2006 as observed by the INSTANT program. *Dyn. Atmos. Oceans* **50**, 115–128 (2010).
15. Beal, L. M., Chereskin, T. K., Lenn, Y. D. & Elipot, S. The sources and mixing characteristics of the Agulhas Current. *J. Phys. Oceanogr.* **36**, 2060–2074 (2006).
16. Guerra, L. A. A., Mill, G. N. & Paiva, A. M. Observing the spread of Agulhas Leakage into the Western South Atlantic by tracking mode waters within ocean rings. *Front. Mar. Sci.* **9**, 958733 (2022).
17. Drijfhout, S. S., Donners, J., & Ruijter de, W. P. M. The origin of intermediate and subpolar mode waters crossing the Atlantic equator in OCCAM. *Geophys. Res. Lett.* **32**, L06602 (2005).
18. Gordon, A. L. Interocean exchange of thermocline water. *J. Geophys. Res. Oceans* **91**, 5037–5046 (1986).
19. Peeters, F. J. C. et al. Vigorous exchange between the Indian and Atlantic oceans at the end of the past five glacial periods. *Nature* **430**, 661–665 (2004).

20. Caley, T., Giraudeau, J., Malaiz,, B., Rossignol, L. & Pierre, C. Agulhas Leakage as a key process in the modes of Quaternary climate changes. *Proc. Natl Acad. Sci. USA* **109**, 6835–6839 (2012).
21. Dyez, K. A., Zahn, R. & Hall, I. R. Multicentennial Agulhas Leakage variability and links to North Atlantic climate during the past 80,000 years. *Paleoceanography* **29**, 1238–1248 (2014).
22. Bard, E. & Rickaby, R. E. M. Migration of the subtropical front as a modulator of glacial climate. *Nature* **460**, 380–383 (2009).
23. Biastoch, A., Böning, C. W., Schwarzkopf, F. U. & Lutjeharms, J. R. E. Increase in Agulhas Leakage due to poleward shift of Southern Hemisphere westerlies. *Nature* **462**, 495–498 (2009).
24. Knorr, G. & Lohmann, G. Rapid transitions in the Atlantic thermohaline circulation triggered by global warming and meltwater during the last deglaciation. *Geochem. Geophys. Geosystems* **8**, Q12006 (2007).
25. Knorr, G. & Lohmann, G. Southern Ocean origin for the resumption of Atlantic thermohaline circulation during deglaciation. *Nature* **424**, 532–536 (2003).
26. Simon, M. H. et al. Salt exchange in the Indian–Atlantic Ocean Gateway since the Last Glacial Maximum: a compensating effect between Agulhas Current changes and salinity variations? *Paleoceanography* **30**, 1318–1327 (2015).
27. Nuber, S. et al. Indian Ocean salinity build-up primes deglacial ocean circulation recovery. *Nature* **617**, 306–311 (2023).
28. Starr, A. et al. Antarctic icebergs reorganize ocean circulation during Pleistocene glacials. *Nature* **589**, 236–241 (2021).
29. Adkins, J. F., McIntyre, K. & Schrag, D. P. The salinity, temperature, and $\delta^{18}O$ of the glacial deep ocean. *Science* **298**, 1769–1773 (2002).
30. Insua, T. L., Spivack, A. J., Graham, D., D'Hondt, S. & Moran, K. Reconstruction of Pacific Ocean bottom water salinity during the Last Glacial Maximum. *Geophys. Res. Lett.* **41**, 2914–2920 (2014).
31. Roberts, J. et al. Evolution of South Atlantic density and chemical stratification across the last deglaciation. *Proc. Natl Acad. Sci. USA* **113**, 514–519 (2016).
32. Knorr, G. et al. A salty deep ocean as a prerequisite for glacial termination. *Nat. Geosci.* **14**, 930–936 (2021).
33. Ferrari, R. et al. Antarctic sea ice control on ocean circulation in present and glacial climates. *Proc. Natl Acad. Sci. USA* **111**, 8753–8758 (2014).
34. Bouttes, N., Paillard, D. & Roche, D. M. Impact of brine-induced stratification on the glacial carbon cycle. *Clim. Past* **6**, 575–589 (2010).
35. Monnin, E. et al. Atmospheric CO_2 concentrations over the last glacial termination. *Science* **291**, 112–114 (2001).
36. Marchitto, T. M., Lehman, S. J., Ortiz, J. D., Flückiger, J. & van Geen, A. Marine radiocarbon evidence for the mechanism of deglacial atmospheric CO_2 rise. *Science* **316**, 1456–1459 (2007).
37. Bryan, S. P., Marchitto, T. M. & Lehman, S. J. The release of ^{14}C-depleted carbon from the deep ocean during the last deglaciation: evidence from the Arabian Sea. *Earth Planet. Sci. Lett.* **298**, 244–254 (2010).
38. Stott, L., Timmermann, A. & Thunell, R. Southern Hemisphere and deep-sea warming led deglacial atmospheric CO_2 rise and tropical warming. *Science* **318**, 435–438 (2007).
39. Spero, H. J. & Lea, D. W. The cause of carbon isotope minimum events on glacial terminations. *Science* **296**, 522–525 (2002).
40. Schiraldi, B., Sikes, E. L., Elmore, A. C., Cook, M. S. & Rose, K. A. Southwest Pacific subtropics responded to last deglacial warming with changes in shallow water sources. *Paleoceanography* **29**, 595–611 (2014).
41. King, A. L. & Howard, W. R. Seasonality of foraminiferal flux in sediment traps at Chatham Rise, SW Pacific: implications for paleotemperature estimates. *Deep Sea Res. Part I* **48**, 1687–1708 (2001).
42. Northcote, L. C. & Neil, H. L. Seasonal variations in foraminiferal flux in the Southern Ocean, Campbell Plateau, New Zealand. *Mar. Micropaleontol.* **56**, 122–137 (2005).
43. Sikes, E. L. et al. Southern Ocean glacial conditions and their influence on deglacial events. *Nat. Rev. Earth Environ.* https://doi.org/10.1038/s43017-023-00436-7 (2023).
44. LeGrande, A. N. & Schmidt, G. A. Global gridded data set of the oxygen isotopic composition in seawater. *Geophys. Res. Lett.* **33**, L12604 (2006).
45. Lambeck, K., Rouby, H., Purcell, A., Sun, Y. & Sambridge, M. Sea level and global ice volumes from the Last Glacial Maximum to the Holocene. *Proc. Natl Acad. Sci. USA* **111**, 15296–15303 (2014).
46. Marr, J. P. et al. Ecological and temperature controls on Mg/Ca ratios of *Globigerina bulloides* from the southwest Pacific Ocean. *Paleoceanography* **26**, PA2209 (2011).
47. Cléroux, C. et al. Mg/Ca and Sr/Ca ratios in planktonic foraminifera: proxies for upper water column temperature reconstruction. *Paleoceanography* **23**, PA3214 (2008).
48. Bemis, B. E., Spero, H. J., Bijma, J. & Lea, D. W. Reevaluation of the oxygen isotopic composition of planktonic foraminifera: experimental results and revised paleotemperature equations. *Paleoceanography* **13**, 150–160 (1998).
49. Grant, K. M. et al. Rapid coupling between ice volume and polar temperature over the past 150,000 years. *Nature* **491**, 744–747 (2012).
50. Glaubke, R. H., Wagner, A. J. & Sikes, E. L. Characterizing the stable oxygen isotopic composition of the southeast Indian Ocean. *Mar. Chem.* **262**, 104397 (2024).
51. Holloway, M. D., Sime, L. C., Singarayer, J. S., Tindall, J. C. & Valdes, P. J. Reconstructing paleosalinity from $\delta^{18}O$: coupled model simulations of the Last Glacial Maximum, last interglacial and Late Holocene. *Quat. Sci. Rev.* **131**, 350–364 (2016).
52. Thirumalai, K., Quinn, T. M. & Marino, G. Constraining past seawater $\delta^{18}O$ and temperature records developed from foraminiferal geochemistry. *Paleoceanography* **31**, 1409–1422 (2016).
53. Gray, W. R. et al. The effects of temperature, salinity, and the carbonate system on Mg/Ca in *Globigerinoides ruber* (white): a global sediment trap calibration. *Earth Planet. Sci. Lett.* **482**, 607–620 (2018).
54. Saenger, C. P. & Evans, M. N. Calibration and validation of environmental controls on planktic foraminifera Mg/Ca using global core-top data. *Paleoceanogr. Paleoclimatol.* **34**, 1249–1270 (2019).
55. Maze, G. & Balem, K. argopy: a Python library for Argo ocean data analysis. *J. Open Source Software* **5**, 2425 (2020).
56. Umling, N. E., Sikes, E., Rafter, P., Goodkin, N. F. & Southon, J. R. Deglacial carbon escape from the northern rim of the Southern Ocean. *Geophys. Res. Lett.* **51**, e2023GL106413 (2024).
57. Pilgrim, C. Piecewise-regression (aka segmented regression) in Python. *J. Open Source Software* **6**, 3859 (2021).
58. Bharti, N. et al. Evidence of poorly ventilated deep central Indian Ocean during the last glaciation. *Earth Planet. Sci. Lett.* **582**, 117438 (2022).
59. Sikes, E. L., Elmore, A. C., Allen, K. A., Cook, M. S. & Guilderson, T. P. Glacial water mass structure and rapid $\delta^{18}O$ and $\delta^{13}C$ changes during the last glacial termination in the Southwest Pacific. *Earth Planet. Sci. Lett.* **456**, 87–97 (2016).
60. Sikes, E. L., Samson, C. R., Guilderson, T. P. & Howard, W. R. Old radiocarbon ages in the southwest Pacific Ocean during the last glacial period and deglaciation. *Nature* **405**, 555–559 (2000).
61. Pang, X., Bassinot, F. & Sepulcre, S. Indonesian Throughflow variability over the last two glacial-interglacial cycles: evidence from the eastern Indian Ocean. *Quat. Sci. Rev.* **256**, 106839 (2021).
62. Wang, X. et al. Precession-paced thermocline water temperature changes in response to upwelling conditions off southern Sumatra over the past 300,000 years. *Quat. Sci. Rev.* **192**, 123–134 (2018).
63. Xu, J., Holbourn, A., Kuhnt, W., Jian, Z. & Kawamura, H. Changes in the thermocline structure of the Indonesian outflow during terminations I and II. *Earth Planet. Sci. Lett.* **273**, 152–162 (2008).

64. Rohling, E. J. Glacial conditions in the Red Sea. *Paleoceanography* **9**, 653–660 (1994).
65. Arz, H. W., Pätzold, J., Müller, P. J. & Moammar, M. Influence of Northern Hemisphere climate and global sea level rise on the restricted Red Sea marine environment during termination I. *Paleoceanography* **18**, 1053 (2003).
66. Sebille van, E., Biastoch, A., Leeuwen van, P. J. & Ruijter de, W. P. M. A weaker Agulhas Current leads to more Agulhas Leakage. *Geophys. Res. Lett.* **36**, L03601 (2009).
67. Martínez-Méndez, G. et al. Contrasting multiproxy reconstructions of surface ocean hydrography in the Agulhas Corridor and implications for the Agulhas Leakage during the last 345,000 years. *Paleoceanography* **25**, PA4227 (2010).
68. Gray, W. R. et al. Poleward shift in the Southern Hemisphere westerly winds synchronous with the deglacial rise in CO_2. *Paleoceanogr. Paleoclimatol.* **38**, e2023PA004666 (2023).
69. Sikes, E. L. & Guilderson, T. P. Southwest Pacific Ocean surface reservoir ages since the last glaciation: circulation insights from multiple-core studies. *Paleoceanography* **31**, 298–310 (2016).
70. Zhang, X., Lohmann, G., Knorr, G. & Xu, X. Different ocean states and transient characteristics in Last Glacial Maximum simulations and implications for deglaciation. *Clim. Past* **9**, 2319–2333 (2013).
71. Sloyan, B. M. & Rintoul, S. R. The Southern Ocean limb of the global deep overturning circulation. *J. Phys. Oceanogr.* **31**, 143–173 (2001).
72. Talley, L. D., Pickard, G. L., Emery, W. J. & Swift, J. H. *Descriptive Physical Oceanography* 6th edn (Elsevier, 2011); https://doi.org/10.1016/b978-0-7506-4552-2.10013-7
73. Phillips, H. E. et al. Progress in understanding of Indian Ocean circulation, variability, air–sea exchange, and impacts on biogeochemistry. *Ocean Sci.* **17**, 1677–1751 (2021).
74. Wong, A. P. S. Subantarctic Mode Water and Antarctic Intermediate Water in the South Indian Ocean based on profiling float data 2000–2004. *J. Mar. Res.* **63**, 789–812 (2005).
75. Lam, A. R. & Leckie, R. M. Late Neogene and Quaternary diversity and taxonomy of subtropical to temperate planktic foraminifera across the Kuroshio Current Extension, northwest Pacific Ocean. *Micropaleontology* **66**, 177–268 (2020).

Methods

Age model

The age model for 50GGC is constrained by aligning the $\delta^{18}O$ record of surface-dwelling *G. bulloides* to Antarctic temperature and $\delta^{18}O$ events in the EPICA Dome C and Dome Fuji ice cores[56]. Both ice cores' chronologies are synchronized to the layer-counted West Antarctic Ice Sheet Divide ice core age model[76]. In the Holocene, where there are fewer Antarctic temperature and $\delta^{18}O$ features to align, radiocarbon dates from planktic foraminifera *Globorotalia inflata* were used for additional age control. Radiocarbon analyses were performed at the Keck Carbon Cycle AMS facility at the University of California, Irvine, and converted to calendar ages using the Bayesian age–depth modelling software BACON version 2.5.7 (ref. 77) using a mean reservoir age of 442 ± 101 years estimated from the Kerguelen Islands[78].

Sample analysis

Globigerina bulloides (250–355 µm) and *Globorotalia truncatulinoides* (355–500 µm; sinistral) were sampled from 50GGC every 1–2 cm throughout the Holocene and deglaciation and every 2–4 cm in the glacial. For stable isotope analyses, 5–10 shells from each species were sonicated, crushed and analysed on a Finnigan MAT-253 Plus isotope ratio mass spectrometer with a Kiel IV device at the City University of New York Advanced Science Research Center's Laboratory for Chemical and Isotopic Signatures. All measurements are reported as a per-mille deviation from the Vienna PeeDee Belemnite standard. Long-term analytical precision, based on the repeated measurement of the NBS-19 standard, was 0.05‰ (1σ; $n = 13$).

The remaining sample material was reserved for trace element analyses. Foraminifera were weighed, crushed and cleaned of authigenic and organic contaminants according to previously established protocols[78]. *G. bulloides* and *G. truncatulinoides* were run on an Element XR high-resolution inductively coupled plasma mass spectrometer at Cardiff University and Old Dominion University, respectively. At Cardiff University, the repeatability of an internal consistency standard with a Mg/Ca ratio of 2.45 mmol mol^{-1} was 0.6% (1σ; $n = 12$). At Old Dominion University, the repeatability of three internal standards with Mg/Ca ratios of 1.44, 3.53 and 5.77 mmol mol^{-1} was 2.86%, 0.65% and 1.25%, respectively (1σ; $n = 6$). All *G. truncatulinoides* were also run in duplicate to assess inter-sample reproducibility, yielding an average replicate error of ±0.11 mmol mol^{-1}. Repeated analyses of the National Institute of Standards and Technology (NIST) RM8301 foraminiferal carbonate standard at Old Dominion University yielded an average Mg/Ca ratio of 2.52 mmol mol^{-1} ($n = 4$) with a precision of 0.15%, in agreement with expected values at 2.62 ± 0.14 mmol mol^{-1} (ref. 79). Analysis of the Cardiff internal standard at Old Dominion University revealed an ~0.13 mmol mol^{-1} offset between the two instruments. We applied a static correction to the *G. bulloides* Mg/Ca ratios from Cardiff to bring them in line with the externally standardized data from Old Dominion.

Estimating temperature and salinity

Past ocean temperatures (T) were estimated from each species' Mg/Ca ratio using the following species- and morphotype-specific calibration equations[46,47]:

$$G.\ bulloides\text{: } \mathrm{Mg/Ca} = 0.955\mathrm{e}^{0.068T}$$

$$G.\ truncatulinoides\text{: } \mathrm{Mg/Ca} = 0.88\mathrm{e}^{0.045T}$$

We selected these equations because they yielded core-top temperature estimates that best resembled modern temperatures at each species' living depth during their preferred growth season (Supporting Information).

Past ocean salinities (S) were estimated by correcting each species' $\delta^{18}O$ record for the influence of temperature and global ice volume. For *G. bulloides*, the temperature correction was performed using a species-specific equation developed in culture[48]. For *G. truncatulinoides*, we applied an equation developed for *Orbulina universa* (low light)[48] that has been successfully applied to *G. truncatulinoides* in the past (for example, refs. 80–82):

$$G.\ bulloides\text{: } (\delta^{18}O_c - \delta^{18}O_{sw} + 0.27) = (T - 13.2)/-4.89$$

$$G.\ truncatulinoides\text{: } (\delta^{18}O_c - \delta^{18}O_{sw} + 0.27) = (T - 16.5)/-4.80$$

A manual correction of +0.27‰ is included to convert from the Vienna PeeDee Belemnite standard to Standard Mean Ocean Water[83]. To account for the ice volume effect, isotopically light $\delta^{18}O$ is added back in reference to a high-resolution record of eustatic sea level (SL) spanning the deglaciation[49] assuming a constant linear relationship[84]:

$$\delta^{18}O_{sw-ivc} = \delta^{18}O + 0.008 \times SL$$

Finally, $\delta^{18}O_{sw\text{-}ivc}$ can be converted to S using a regional $\delta^{18}O_{sw}$–salinity regression from the subtropical south Indian Ocean[50]:

$$\delta^{18}O_{sw} = 0.503 \times S - 17.21$$

All uncertainties were propagated throughout these systems of equations using the Paleo Seawater Uncertainty Solver algorithm (PSU Solver) for MATLAB[52]. The programme estimates overall uncertainty by iteratively solving all equations while allowing inputted data and sample age to vary within their 1σ uncertainties at each iteration. In this way, errors associated with analytical precision, sample reproducibility (available only for *G. truncatulinoides*), the 50GGC age model and the sea-level curve used for ice volume corrections are constrained probabilistically at each time step. For our applications, the number of Monte Carlo iterations was set to $n = 5{,}000$. The temperature, $\delta^{18}O_{sw\text{-}ivc}$ and salinity values presented in the paper represent median estimates across all Monte Carlo realizations bounded by the 32nd–68th (1σ) and 5th–95th (2σ) percentiles. These uncertainties are slightly skewed from a standard normal distribution, so for simplicity we report uncertainty in the text as the mean 1σ error across the full length of the records using the equation below:

$$\bar{\sigma} = \frac{\sum_{i=1}^{n}\left(\frac{\sigma^{+}+\sigma^{-}}{2}\right)}{n}$$

where σ^{+} and σ^{-} represent the positive and negative errors, respectively, and n is the number of datapoints in the record.

Changepoint analyses and pairwise comparisons

To quantify the onset of deglacial change in 50GGC and other previously published records, we use a piecewise regression approached developed in Python[57]. The method starts with an initial guess on the location of a changepoint before iteratively solving a series of multivariate Taylor expansions, eventually converging on changepoint estimates. This technique is not guaranteed to identify a globally optimum estimate, and so the algorithm adopts a Monte Carlo framework to generate multiple realizations of its changepoint estimates. For our purposes, the number of Monte Carlo realizations was set to $n = 5{,}000$. The changepoints we report are the mean and $\pm1\sigma$ of these realizations. Estimates are also sensitive to the number of expected changepoints defined before analysis. Given that there are several features in our records that could be considered changepoints (for example, the beginning, peak and termination of the high-salinity event), we assigned the number of expected changepoints to be three. Some longer records were trimmed to the period under investigation (0–30 ka) to focus analysis on the Last Deglaciation. Under these conditions, the onset of deglacial change was consistently identified in all records with no other changepoints falling with ±2 ka. Significant

differences between changepoints across records were determined using a simple two sample two-tailed *z*-test with a 95% confidence threshold ($\alpha = 0.05$).

Estimating negative freshwater forcing

To estimate the amount of freshwater that would need to be removed from glacial SAMW to explain the deglacial salinity increase observed at 50GGC, we use a basic dilution equation:

$$S_{LGM} V_{LGM} = S_{HSE} V_{HSE}$$

where S and V represent the salinities and mode water volume transport, respectively, for the Last Glacial Maximum (LGM) and the High-Salinity Event (HSE). For simplicity, we treat the problem as if we were diluting HSE waters with freshwater to match the lower salinities of the LGM. This is effectively the same amount of freshwater that would need to be removed to increase glacial salinities to those of the HSE, just with the opposite sign.

We rearrange the equation above to solve for the total volume transport during the LGM (V_{LGM}):

$$V_{LGM} = (S_{HSE} V_{HSE}) / S_{LGM}$$

Average salinities (with 1σ error) were determined by computing the mean and standard deviation from the HSE (16–18 ka) and last glacial period (20–30 ka). For the V_{HSE} term, we use a modern SAMW production of 11.7 Sv (ref. 4) due to the lack of deglacial production estimates. The sensitivity of our calculations to SAMW production rate is shown in Supplementary Fig. 2 and discussed in Supplementary Information. Assuming SAMW production was consistent through time, the difference between the calculated volume transport during the LGM (V_{LGM}) and the SAMW production rate used for the HSE (V_{HSE}) represents the total freshwater flux in Sv (V_{FW}):

$$V_{FW} = V_{LGM} - V_{HSE}$$

Error propagation for these equations was handled using the 'uncertainties' package for Python, version 3.1.7 (ref. 85).

Data availability

The geochemical data from TT1811-50GGC, and the temperature and salinity records derived from them, are archived and accessible through the National Oceanic and Atmospheric Administration (NOAA) National Centers for Environmental Information (https://doi.org/10.25921/j8fc-gh57)[86]. Sediments from TT1811-50GGC are archived at the Oregon State University Marine Geology Repository.

Code availability

Code for visualizing 50GGC data and reproducing our changepoint analyses is available on Zenodo at https://doi.org/10.5281/zenodo.15283459 (ref. 87). The programme used to convert our geochemical data into reconstructed temperatures and salinities can be found on the MATLAB Central File Exchange at https://ch.mathworks.com/matlabcentral/fileexchange/59565-paleo-seawater-uncertainty-solver.

References

76. Buizert, C. et al. Abrupt ice-age shifts in southern westerly winds and Antarctic climate forced from the north. *Nature* **563**, 681–685 (2018).
77. Blaauw, M. & Christen, J. A. Flexible paleoclimate age-depth models using an autoregressive gamma process. *Bayesian Anal.* **6**, 457–474 (2011).
78. Lea, D. W., Pak, D. K. & Spero, H. J. Climate impact of Late Quaternary equatorial Pacific sea surface temperature variations. *Science* **289**, 1719–1724 (2000).
79. Stewart, J. A. et al. NIST RM 8301 boron isotopes in marine carbonate (simulated coral and foraminifera solutions): inter-laboratory $\delta^{11}B$ and trace element ratio value assignment. *Geostand. Geoanal. Res.* **45**, 77–96 (2021).
80. LeGrande, A. N., Lynch-Stieglitz, J. & Farmer, E. C. Oxygen isotopic composition of *Globorotalia truncatulinoides* as a proxy for intermediate depth density. *Paleoceanography* **19**, PA4025 (2004).
81. Parker, A. O., Schmidt, M. W. & Chang, P. Tropical North Atlantic subsurface warming events as a fingerprint for AMOC variability during Marine Isotope Stage 3. *Paleoceanography* **30**, 1425–1436 (2015).
82. Spear, J. W., Poore, R. Z. & Quinn, T. M. *Globorotalia truncatulinoides* (dextral) Mg/Ca as a proxy for Gulf of Mexico winter mixed-layer temperature: evidence from a sediment trap in the northern Gulf of Mexico. *Mar. Micropaleontol.* **80**, 53–61 (2011).
83. Hut, G. *Stable Isotope Reference Samples for Geochemical and Hydrological Investigations* (Consultant Group Meeting IAEA, 1987).
84. Schrag, D. P. et al. The oxygen isotopic composition of seawater during the Last Glacial Maximum. *Quat. Sci. Rev.* **21**, 331–342 (2002).
85. Lebigot, E. O. *Uncertainties: A Python Package for Calculations with Uncertainties* (PyPI, 2022).
86. Glaubke, R. H. et al. NOAA/WDS paleoclimatology - foraminiferal geochemistry and derived past temperatures and salinities from *G. bulloides* and *G. truncatulinoides* in the South Indian Ocean. *NOAA National Centers for Environmental Information* https://doi.org/10.25921/j8fc-gh57 (2025).
87. Glaubke, R. Elevated shallow water salinity in the deglacial Indian Ocean was sourced from the deep. *Zenodo* https://doi.org/10.5281/zenodo.15283459 (2025).

Acknowledgements

We thank C. Spencer Jones and two anonymous reviewers for their insightful comments on earlier drafts of this paper. We are grateful to the captain, crew and sea-going scientists aboard the R/V *Thomas G. Thompson* for their help collecting samples during the CROCCA-2S expedition (TN362). We also wish to acknowledge B. Sohst, B. Giebel, M. Nairn and S. Slater for their assistance with geochemical analyses. This work was supported by the National Science Foundation (grants OCE 1559080, OCE 1940962 and OCE 2002642 awarded to E.L.S. and OCE 2002630 awarded to N.E.U.).

Author contributions

All members of the authorship team contributed substantially to this work. R.H.G. conceived of the study with E.L.S., processed and analysed samples, developed the code for data analysis and visualization, interpreted the data, and wrote the paper. E.L.S. contributed to project development, data interpretation, funding acquisition and writing the paper. S.M.S., N.E.U., A.S. and P.L.M.-S. helped process and analyse samples, provided insight on data interpretation, and edited the paper. N.E.U. also contributed to funding acquisition. A.S. helped develop the negative freshwater forcing calculations. M.W.S. provided lab space and materials and edited the paper.

Competing interests

The authors declare no competing interests.

Additional information

Supplementary information The online version contains supplementary material available at https://doi.org/10.1038/s41561-025-01756-7.

Correspondence and requests for materials should be addressed to Ryan H. Glaubke.

Peer review information *Nature Geoscience* thanks C. Spencer Jones and the other, anonymous, reviewer(s) for their contribution to the peer review of this work. Primary Handling Editor: James Super, in collaboration with the *Nature Geoscience* team.